Signatures of Dark Matter Halo Expansion in Galaxy Populations

Chris B. Brook[1]* & Arianna Di Cintio[2]

[1]*Ramon y Cajal Fellow, Departamento de Física Teórica, Universidad Autónoma de Madrid, 28049 Cantoblanco, Madrid, Spain*
[2]*Dark Fellow, Dark Cosmology Centre, NBI, University of Copenhagen, Juliane Maries Vej 30, DK-2100 Copenhagen, Denmark*

ABSTRACT

Dark matter cores within galaxy haloes can be formed by energy feedback from star forming regions: an energy balance suggests that the maximum *core formation efficiency* arises in galaxies with $M_{star} \sim 10^{8.5} M_{\odot}$. We show that a model population of galaxies, in which the density profile has been modified by such baryonic feedback, is able to explain the observed galaxy velocity function and Tully-Fisher relations significantly better than a model in which a universal cuspy density profile is assumed.

Alternative models, namely warm or self-interacting dark matter, also provide a better match to these observed relations than a universal profile model does, but make different predictions for how halo density profiles vary with mass compared to the baryonic feedback case. We propose that different core formation mechanisms may be distinguished based on the imprint they leave on galaxy populations over a wide range of mass.

Within the current observational data we find evidence of the expected signatures of the mass dependence of core formation generated by baryonic feedback.

Key words: galaxies: evolution - formation - haloes cosmology: theory - dark matter

1 INTRODUCTION

The rotational velocity of gas and stars in galaxy discs implies that galaxies are embedded within dark matter 'haloes'. A central tenet of the canonical cold dark matter (ΛCDM) cosmological model is that such haloes have dense central regions with steep, "cuspy" inner density profiles (Navarro et al. 1996b, hereafter NFW profile). However, observed rotation curves imply that dwarf galaxies have flat "cores" at their centre (Moore 1994). This "cusp-core" crisis is a major challenge to the ΛCDM paradigm, heightened by studies which demonstrate that some non-standard dark matter particles form cored haloes (Macciò et al. 2012; Vogelsberger et al. 2012).

On the other hand, astrophysical processes (Navarro et al. 1996a; Pontzen & Governato 2012) within a cold dark matter framework may modify halo density profiles and create cored haloes at specific halo masses (Di Cintio et al. 2014a). While observed rotation curves of individual galaxies provide compelling evidence for the existence of cores in low surface brightness and dwarf galaxies (Oh et al. 2011), they are not able to distinguish between the various proposed origins of cores. Therefore, it is essential to establish whether the "cusp-core" crisis is pointing to a

new cosmological paradigm, or is instead the result of astrophysical processes within the standard ΛCDM model.

In the ΛCDM paradigm, cores may result from the non-adiabatic impact of gas outflows on dark matter haloes. There is significant evidence (Weiner et al. 2009; Martin et al. 2012) that energy feedback from star-formation activity drives gas out of galaxies, and that processes such as radiation energy from massive stars, stellar winds and supernova explosions are important in galaxy formation (e.g. Brook et al. 2011). The degree to which such energetic processes flatten the inner density profiles of haloes depends on the ratio of their stellar to halo masses (Di Cintio et al. 2014a, see Section 2 for an analytic argument).

Low mass galaxies are dark matter dominated: those with $M_{star} \lesssim 3 \times 10^6 M_{\odot}$ do not produce enough energy to flatten their halo's inner density profile, which remains steep (Peñarrubia et al. 2012; Governato et al. 2012). As stellar mass increases relative to the dark matter mass, the inner density profile becomes increasingly flat (Governato et al. 2012). The flattening is greatest when $M_{star} \sim 3 \times 10^8 M_{\odot}$, after which the increasingly deep potential well is able to oppose halo expansion resulting in less flattening for more massive galaxies (Di Cintio et al. 2014a).

One approach to test core formation by baryonic processes has been to study low mass dwarf galaxies, where the theory predicts cuspy, NFW profiles. A multitude of studies have attempted to determine whether galaxies such as Sculptor have a core (Battaglia et al. 2008; Walker et al. 2009; Evans et al. 2009; Walker & Peñarrubia 2011; Agnello & Evans 2012; Amorisco & Evans 2012;

---

* E-mail: cbabrook@gmail.com

Laporte et al. 2013; Adams et al. 2014; Strigari et al. 2014), without a clear consensus emerging.

In this study, we therefore take another approach and explore the properties of an ensemble of galaxies. We show that the mass dependence of cores formed through baryonic processes should leave an imprint on galaxy populations, and that such imprint may be used to distinguish between different core formation mechanisms. Indeed, while alternative dark matter particles could also be able to create cores, they would result in a different dependence of core sizes versus galaxy mass.

In particular, we study the velocity function of galaxies (Zavala et al. 2009; Zwaan et al. 2010; Trujillo-Gomez et al. 2011; Papastergis et al. 2011; Obreschkow et al. 2013; Klypin et al. 2014), as well as the relation between velocity and stellar mass (Tully & Fisher 1977), over a wide mass range in which core sizes are expected to vary in different ways according to different models.

To model haloes that are flattened by energetic feedback processes, we use the mass dependent density profile (Di Cintio et al. 2014b), hereafter DC14 profile, in which galaxies with M_{star} between $\sim 3 \times 10^6$ and $\sim 10^{10}$ $M_\odot$ have central densities shallower than the NFW profile (Di Cintio et al. 2014a). The DC14 model has already been used to study the variation in core sizes for Local Group dwarf galaxies, in which their observed kinematics has been explained in terms of a density profile dependent on M_{star}/M_{halo} (Brook & Di Cintio 2015).

Standard alternative dark matter models, in particular a warm dark matter (WDM) and a self interacting dark matter (SIDM) one, are also explored and the expected properties of galaxy populations within such models are compared with the fiducial NFW model. We highlight the manner in which the alternative dark matter models presented can be generalized to a wide range of parameterizations.

In Section 2 we present the ingredients of our models, including an analytic argument for our expectation of how core sizes vary with mass in the baryonic feedback scenario. In Section 3 we create velocity distribution functions of galaxies and M_{star}-velocity relations, and we compare the predictions coming from the DC14 model to the results obtained by using a standard NFW model (Sections 3.1 and 3.2). We also compare velocity functions and M_{star}-velocity relations for the alternative dark matter models, namely WDM and SIDM (Section 3.3). We discuss possible uncertainties and caveats in Section 3.4 and 3.5. In Section 4 we show that the different models result in different observational trends with mass within galaxy populations, and that such trends may be distinguishable with careful observations.

2   INGREDIENTS OF OUR MODELS

Our models consist of a mass function for dark matter haloes with appropriate concentrations, a relation between stellar and halo mass, and exponential stellar and gas discs. Dark matter haloes are modelled by different density profiles, as explained below. Halo mass distributions for ΛCDM and WDM assume Planck cosmological parameters and are created with `HMFcalc` (Murray et al. 2013), with appropriate corrections to the WDM mass function (Schneider et al. 2012). The WDM model has a particle mass of 2 KeV, with the effect of using 1, 2 & 3 KeV particles shown in section 3.3.1.

We use the concentration-mass relation from Planck ΛCDM (Dutton & Macciò 2014), and adjust the WDM halo concentration (Schneider et al. 2012). An adiabatic contraction correction to the dark matter haloes is applied to all models, as found in cosmo-
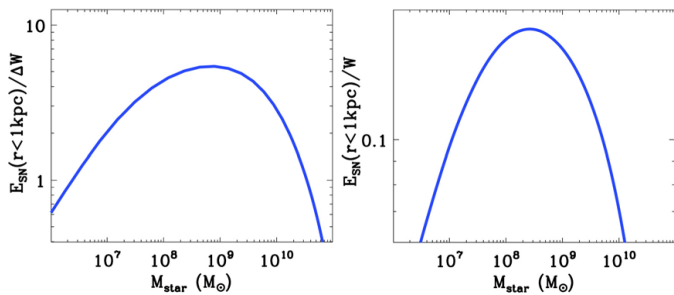
Figure 1. Left Panel:The ratio of supernova energy from stars within the central 1 kpc, $E_{SN}(r<1\,kpc)$, and the energy required to transform an NFW profile to a profile with a 1 kpc core (ΔW), plotted as a function of M_{star}. Only galaxies in the mass range, $3 \times 10^6 \lesssim M_{star} \lesssim 10^{10} M_\odot$ have sufficient energy to form cores. Right Panel: The ratio of supernova energy from stars within the central 1 kpc, and the potential of an NFW profile with embedded baryonic disk

as a function of M_{star}. This ratio gives an indication of the efficiency of core formation: one expects the largest cores at $M_{star} \sim 3 \times 10^8 M_\odot$.

logical simulations for galaxies as massive as the Milky Way (Di Cintio et al. 2014b). Such contraction alters the concentration (i.e. the scale radius) rather than the inner slope, allowing core sizes to be set. Specifically we use

$$C = (1.0 + 0.00001 e^{3.4X}) \times C_{NFW} \qquad (1)$$

where $X = \log_{10}(M_{star}/M_{halo}) + 4.5$, and C_{NFW} is the concentration given from the adopted (Dutton & Macciò 2014) relation.

Haloes are matched to galaxy stellar masses using the empirical abundance matching relation of Guo et al. (2010). We explore the effects of different abundance matching relations in Section 3.5.

Once a relation between dark matter halo mass and galaxy stellar mass has been set, we add a stellar exponential disc with scale-length h_s taken from the observed M_{star}-h_s relation, $\log_{10}h_s = -2.462 + 0.281\log_{10}M_{star}$ (equation 7 in Dutton et al. (2011a)). We further add a gas disk with mass $M_{gas} = 1.3M_{HI}$, with $\log_{10}(M_{HI}/M_{star}) = -0.43\log_{10}M_{star} + 3.75$ (Papastergis et al. 2012) and disc scale length $h_g = 3h_s$.

The circular velocity of a thin exponential disk of mass M_d and scale length h_i is given by:

$$V_{disk}^2(r) = \frac{GM_d}{h_i} 2y^2 [I_0(y)K_0(y) - I_1(y)K_1(y)] \qquad (2)$$

where $y = r/(2h_i)$ and I_n, K_n are modified Bessel functions (Dutton et al. 2011b).

In all models we include the universal dark matter fraction of mass ($\Omega_{DM}/\Omega_m = 0.85$) in dark matter haloes. The density profile of dark matter haloes is set to be either the universal, NFW one (Navarro et al. 1996b), or the mass-dependent DC14 density profile described in the next section (Di Cintio et al. 2014b).

WDM halos are known to have cored profiles (Tremaine & Gunn 1979; Bode et al. 2001). However, Macciò et al. (2012) find that WDM particles with the masses considered in our study, 1-3KeV, result in very small cores of order 10pc for halos of mass $10^{10}M_\odot$, and that it requires much lower mass (~ 0.1KeV) WDM particles to create cores of 1 kpc. In this study, we approximate the very small cores of WDM halos in our model by retaining the NFW profile.

In the adopted SIDM model, core sizes are set to zero for Milky Way mass galaxies ($M_{star} = 6 \times 10^{10} M_\odot$) and increases as

the scale-length decreases, until reaching a core size of 1 kpc for $M_{star}=10^8 M_\odot$ (Vogelsberger et al. 2012, 2014). Lower mass haloes all have core sizes of 1 kpc. Other parameterizations for varying core sizes are explored in section 3.3.2. Of course, they do not cover all SIDM models and it is possible to fine tune SIDM parameters in order to have a mass variation of halo profile similar to the one of baryonic outflow models. On the other hand, the parameterisations that we do explore here can be generalized, since they are representative of a range of alternative dark matter candidates that predict similar behaviour of core size with galaxy mass. Cored profiles of dark matter for the SIDM case take the form:

$$\rho(r) = \frac{\rho_0 r_{scale}^3}{(r_c + r)(r_{scale} + r)^2} \qquad (3)$$

where ρ_0 is a characteristic halo density, r_{scale} is a scale radius and r_c is the core size (Peñarrubia et al. 2012). The velocity profile of dark matter haloes, V_{DM}, will thus depend on the type of density profile chosen. The theoretical, total circular velocity profile of a galaxy at any radius, defined as V_{rot}, is therefore given by the quadratic sum of the circular velocities of the various components:

$$V_{rot}(r) = \sqrt{V_{star}^2(r) + V_{gas}^2(r) + V_{DM}^2(r)} \qquad (4)$$

2.1 The mass dependent 'DC14' profile

The analytic work in this section follows the work of Peñarrubia et al. (2012) who model the balance between the gravitational potential of galaxies and the energy from central star formation regions as the main determinant of core formation in the case of cores created by astrophysical processes (Peñarrubia et al. 2012). Once an exponential stellar and gas discs have been set as explained above, using observed scaling relations (Dutton et al. 2011a; Fathi et al. 2010; Papastergis et al. 2012), it is possible to compute the supernova energy from stars within the central 1 kpc of each galaxy and compare with the depth of its potential well.

The left panel of Figure 1 shows the ratio of such supernova energy, $E_{SN}(r<1\,kpc)$, divided by the gravitational potential energy ΔW required to transform an initially NFW halo to a halo whose profile has a 1 kpc core, plotted as a function of M_{star}. ΔW is defined as $\Delta W=(W_{cusp}-W_{core})/2$, where:

$$W = -4\pi G \int_0^{rvir} \rho(r) M(r) r dr \qquad (5)$$

The supernova energy within 1 Kpc is easily computed by:

$$E_{SN} = M_{star}(<1\mathrm{kpc}) \bar{f}_{SN} \epsilon 10^{51} \mathrm{erg} \qquad (6)$$

where $\bar{f}_{SN}$ is the fraction of stars that will explode as supernovae divided by the mean stellar mass according to the initial mass function selected ($\bar{f}_{SN} = 0.00925$ for a Kroupa (2002) IMF), ϵ is the fraction of energy that will be transferred into the dark matter halo and 10^{51}erg is the energy released during a single supernova event.

Figure 1 assumes that galaxies are connected to dark matter haloes via the abundance matching relation of (Guo et al. 2010). It is clear that only galaxies in the mass range $3\times10^6 \lesssim M_{star} \lesssim \times10^{10} M_\odot$ have sufficient energy to form cores.

The right panel of Figure 1 shows the ratio of supernova energy from stars within the central 1 kpc, and the gravitational potential energy of an NFW halo plus a baryonic disk as a function of M_{star}. This ratio, namely the balance between SNe energy vs potential of the galaxy, gives an indication of the efficiency of core

formation: the largest cores are expected at the peak of this relation, i.e. at $M_{star}\sim3\times10^8 M_\odot$.

In Figure 1 we used $\epsilon = 0.4$, and we note that using different values will simply shift the plots up or down, changing the minimum mass for core formation but without modifying the position of the peak. Whilst we have included only energy from SNe in this calculation, it is likely that ionising radiation will help drive outflows (Murray et al. 2010): again our analytic argument of where we expect the peak of core formation will not be affected, as long as this feedback scales with star formation rate.

We will explore the effects of AGN, which do not scale with star formation rate, later in the paper; for now we just note that the stellar mass where core formation is most efficient is below the mass range where we expect AGN feedback to be important. Bulges have not been included in our models because at the core formation peak mass in Figure 1 most galaxies do not have bulges. Nevertheless, we tested the results of adding empirically motived bulges, following the Hernquist formalism (Hernquist 1990): we found that the only difference is the appearance of a "shoulder" on the right side of the the plots, since more SNe energy is stored within the inner 1 kpc of a galaxy with a bulge, while the peak of core formation does not get affected.

Of course, our model is very simplistic. In particular, Peñarrubia et al. (2012) showed that the energy requirements for core formation are significantly lower at higher redshift. And further, Maxwell et al. (2015) recently showed that the radius to which dark matter is moved when it is expelled from the cusp region, will also have an effect on the energy required to form a core. Yet a very similar relation between core formation and galaxy mass has been found in cosmological simulations (Di Cintio et al. 2014a) of galaxies that match a wide range of galaxy scaling relations (Brook et al. 2012b; Stinson et al. 2013; Kannan et al. 2014; Obreja et al. 2014): within these simulations, the flattest profiles are also found at $M_{star}\sim3\times10^8 M_\odot$.

The mass dependent DC14 density profile is based on such cosmological simulations, and accounts for the expansion of dark matter haloes due to the effects of feedback from star forming regions (Di Cintio et al. 2014b). These profiles self consistently account for the distance to which dark matter is moved, addressing the concerns of Maxwell et al. (2015), and take the form:

$$\rho(r) = \frac{\rho_s}{\left(\frac{r}{r_s}\right)^\gamma \left[1 + \left(\frac{r}{r_s}\right)^\alpha\right]^{(\beta-\gamma)/\alpha}} \qquad (7)$$

where (α, β, γ) indicate the sharpness of the transition, the outer and the inner slope, respectively (Merritt et al. 2006).

The DC14 model describes profiles that have a range of inner slopes, with the parameters of the double power law model being dependent on the stellar-to-halo mass ratio of a galaxy in the following way (Di Cintio et al. 2014b):

$$\begin{aligned} \alpha &= 2.94 - \log_{10}[(10^{X+2.33})^{-1.08} + (10^{X+2.33})^{2.29}] \\ \beta &= 4.23 + 1.34X + 0.26X^2 \\ \gamma &= -0.06 + \log_{10}[(10^{X+2.56})^{-0.68} + (10^{X+2.56})] \end{aligned} \qquad (8)$$

where $X = \log_{10}(M_{star}/M_{halo})$. The scale radius, r_s, is connected to the concentration of the halo, which varies with mass.

As long as the flattening of the central dark matter density is mass dependent, and there is a maximum flattening at a similar stellar mass as found in both the analytic model and the simulations, the exact form of the profile will not affect the arguments presented in this study.
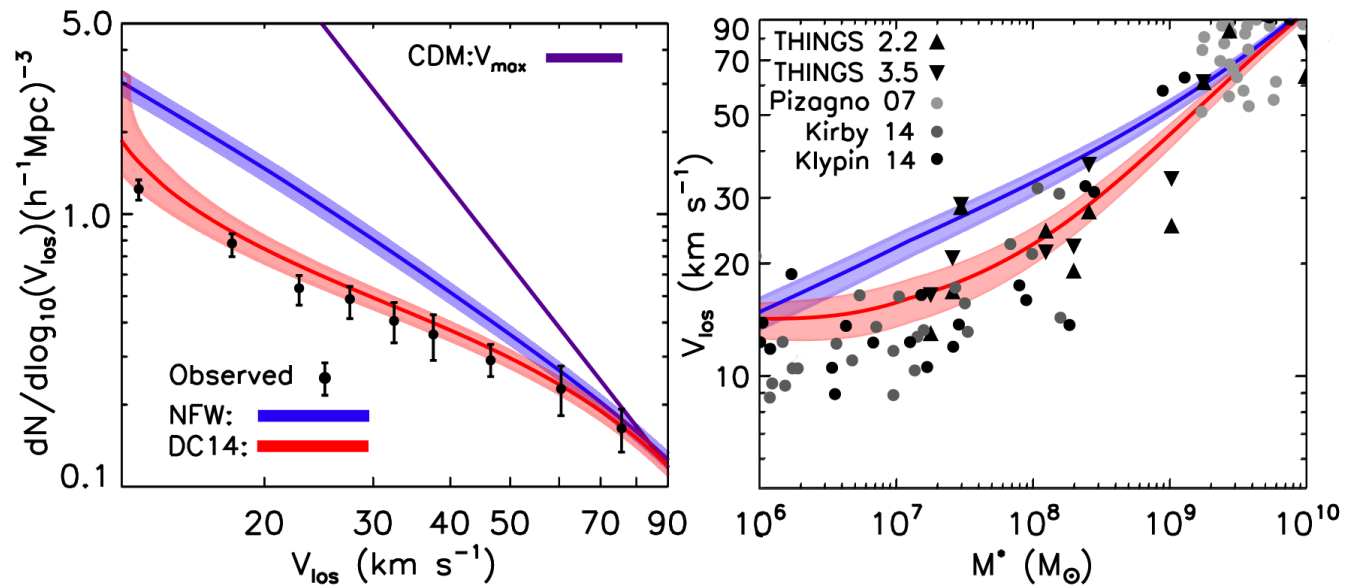
Figure 2. Left Panel: the number of galaxies per line of sight velocity per unit volume, as a function of maximum circular velocity (V_{max}) for CDM theory (purple line) and as a function of V_{los} for observations. The observed distribution of V_{los} is shown as black circles with error bars (Klypin et al. 2014). The V_{los} distribution for a ΛCDM model with NFW and DC14 profiles are shown in blue and red, respectively, with the velocity measured at the radius indicated in Figure 3. Shaded regions show the same distribution using ±20% the radius at which measurements are taken. The mass dependent DC14 profile results in a flattening of the V_{los} distribution, caused by increasingly flat density profiles as we move from disc galaxies with high V_{los} to lower V_{los}. At the lowest, dwarf scales, the density profiles of the DC14 model steepen again, reflected in an upturn at $V_{los} \lesssim 20\,\mathrm{km\,s^{-1}}$, in agreement with observation. Right Panel: The observed (filled symbols) and predicted M_{star}-V_{los} relations for the ΛCDM model with NFW (blue) and DC14 (red) profiles, measured at 2.2 and 3.5 disc scale-lengths with solid line at the midpoint, 2.85 disc scale-lengths. For the DC14 profile, the relation bends down from the standard NFW model at intermediate masses, and then flattens at low stellar masses, providing a match for observed dwarf galaxies.

3   RESULTS

3.1   Velocity Function

When testing theoretical cosmological models, dark matter haloes can be matched to observed galaxies within a given volume (e.g. Guo et al. 2010; Moster et al. 2010; Papastergis et al. 2015). The density profiles of dark matter haloes, together with the above mentioned disk distributions of stars and gas, can be used to determine the theoretical velocity profile of a galaxy at a given radius, V_{rot}, according to Eq.3: such velocity is determined by the total mass of dark matter, gas and stars contained within that radius.

The standard ΛCDM model, in which haloes have cuspy, NFW density profiles (Navarro et al. 1996b), predicts a far greater number of galaxies than are observed with line-of-sight velocity (V_{los}) less than ∼60 km s^{-1} (Zavala et al. 2009; Zwaan et al. 2010; Trujillo-Gomez et al. 2011; Papastergis et al. 2011; Klypin et al. 2014).

This can be seen by comparing the ΛCDM prediction, purple line, to the observational data points (Klypin et al. 2014) in the left panel of Figure 2. The observed V_{los} distributions are taken from compiled data of the of HI line-widths of Local Volume galaxies (Karachentsev et al. 2013) measured at 50% of the maximum intensity, $W50$, with a further accounting for the number of early type galaxies which do not have significant amounts of HI (Klypin et al. 2014).

The comparison is made assuming that the observed velocities of gas within galaxies track the maximum possible velocity associated with the corresponding dark matter halo, V_{max}. The assumption made in Klypin et al. (2014) that observed velocities relate directly to V_{max} may be justified in high mass galaxies, but

is not necessarily correct in less massive galaxies, where the rotation curves are often still increasing at their outermost measured point (Catinella et al. 2006; Swaters et al. 2009; de Blok et al. 2008; Oh et al. 2011). For example, in a dwarf galaxy with stellar mass $M_{star}=10^{7-8}M_{\odot}$, observed velocity measurements often come from stars within 1-2 kpc of the galaxy centre, while the V_{max} of the corresponding NFW halo is at ∼7-10 kpc. If haloes are cored or expanded, then the V_{max} may be even further from the centre of the galaxy: indeed, the maximum observed rotation velocity may be a poor estimate of V_{max} in the case of a cored profile.

In Papastergis et al. (2015) this issue is addressed by attempting to place observed galaxies on the V_{rot}-V_{max} diagram expected from abundance matching, by fitting several dark matter haloes to observed rotation curves and considering only the last measured point of such velocity curves in order to determine the maximum velocity of the most massive halo that fits such point (see also Ferrero et al. (2012)). In this sense, this is a more conservative approach than the one followed by Klypin et al. (2014). However such methodology still assumes that dark matter haloes follow the universal NFW profile, but for some of the observed rotation curves in low mass galaxies this is not the case (see for example UGC7577 in their Fig.5).

Debating whether rotation curves *appear flat* may not be the optimal manner to address the issue of how to best compare theory and observation. Models provide predictions for velocities at all radii, so one can compare observations with theoretical predictions for velocities at any radius, as long as the two are done consistently. This is particularly important when comparing models of different density profiles.

We therefore suggest a different approach, which is to estimate the physical radius at which measurements are made, and then compare models and observations at that same radius. In order to determine the radial region where V_{los} is measured in HI surveys, we find the radius, R_m, at which observed rotation curves reach the inclination and velocity dispersion adjusted value V_{rot}.

In Figure 3 we plot, as black squares, R_m as a function of M_{star} for 26 observed galaxies which have $M_{star} \lesssim 10^{10} M_\odot$, high resolution rotation curves (Oh et al. 2008; de Blok et al. 2008; Oh et al. 2011; Cannon et al. 2011; Oh et al. 2015) and corresponding $W50$ values (Walter et al. 2008). The orange line shows a fit to the data,

$$\log(R_m) = -2.75 + 0.37 \times \log(M_{star}), \qquad (9)$$

with the shaded region indicating $R_m \pm 20\%$. The purple line is the radius R_{max} at which a halo of a specific stellar mass, according to M_{star}-M_{halo} relations, reaches its maximum velocity V_{max}. It is clear how moving toward low mass galaxies the gas is tracking an increasingly inner region of the halo rather than extending to R_{max}. The lower is the mass of a galaxy, the higher is the separation between R_m and R_{max}. We therefore decided to use the radius R_m as the radius where we measure velocities in our theoretical models, to be consistent with observations.

In the left panel of Figure 2, we derived theoretical velocity functions by first assuming a mass function for dark matter haloes, with appropriate halo concentration-mass dependence, then using the density profiles of different models to derive galaxies' circular velocities at each radius. We then measure circular velocities at the radius R_m to mimic the region where observations are made. We remark that before comparing the observed line-of-sight velocity, V_{los}, with the theoretically predicted rotation curve, V_{rot}, a correction must be applied to account for the pressure support of gas in real galaxies. When using HI line widths, $V_{los} = W50/2$, where $W50$ is the width of the HI line profile measured at 50 per cent of the peak value, and the rotational velocity is then:

$$V_{rot} = \sqrt{\left(\frac{V_{los}}{\sin(i)}\right)^2 - \sigma_v^2}, \qquad (10)$$

where i is the inclination of the galaxy and $\sigma_v = 8$ km/s is the typical amplitude of gas turbulent motion, in addition to rotation (Papastergis et al. 2015). In our theoretical velocity function, we average over all possible inclinations. We use equation 10 to transform from circular velocities measured at R_m to V_{los} velocities, and do this self-consistently for all the models, i.e. NFW, DC14, WDM and SIDM.

Using the standard ΛCDM model with associated cuspy, NFW halo density profiles, the model still overpredicts the number of galaxies with $V_{los} \lesssim 60$ km s^{-1}: the theoretical NFW velocity function lies significantly above observations as can be seen from the blue shaded line in Figure 2.

This discrepancy motivates the exploration of other models which may lead to different predictions for the distribution of V_{los} of galaxies. We first explore the mass dependent DC14 density profile, based on simulations where cores are formed through outflows driven by star formation activity, and fully described in Section 2.1.

The theoretical velocity function based on a DC14 profile is shown as a red shaded region in Figure 2 and its agreement with observations is notable. As we move from massive to intermediate mass galaxies, the DC14 profile describes haloes which become increasingly flat in their inner regions, resulting in fewer galaxies with $30 \lesssim V_{los} \lesssim 60$ km s^{-1}, in line with observations.
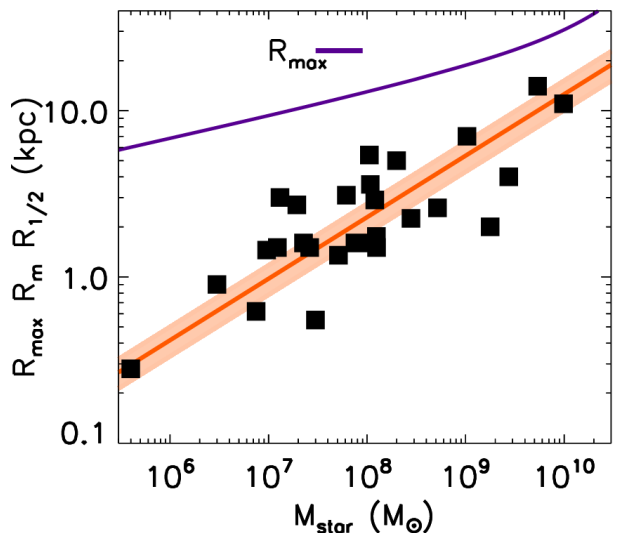
Figure 3. The radius, R_m, at which the observed rotation curves of 26 observed galaxies taken from the literature reach the inclination and velocity dispersion adjusted value $V_{rot} = \sqrt{((W50/2/sin(i))^2 - \sigma_v^2)}$, plotted against stellar mass (black squares). The orange line is a fit to this data, with the shaded region indicating $R_m \pm 20\%$. The purple line is the radius R_{max} at which an halo of a specific stellar mass (Guo et al. 2010) reaches its maximum velocity V_{max}. The discrepancy between R_{max} and R_m is more severe moving toward low mass galaxies.

Below $M_{star} \sim 3 \times 10^8 M_\odot$, the inner region of DC14 profiles become increasingly steep. This results in a slight upward bend at $V_{los} \lesssim 20$ km s^{-1} with the V_{los} distribution eventually joining the standard ΛCDM model for $V_{los} \lesssim 10$ km s^{-1}, where the haloes retain a NFW profile given the insufficient energy from SNe to create a core.

This upward trend in the velocity function at $V_{los} \lesssim 20$ km s^{-1} is a prediction of models in which cores are formed by baryonic outflows, and in which density profiles remain steep in the lowest mass galaxies. Interestingly, the low velocity end of observations also show an upturn, as derived in Klypin et al. (2014) and precisely as predicted by the DC14 model.

Of course, the upturn in the observations needs to be taken with a grain of salt. Indeed, moving to lower masses, observations are less well constrained for two reasons. Firstly, below stellar mass of $\sim 10^9 M_\odot$ the HI disks become on average thicker (Brinks et al. 2002) with the velocity dispersions being a larger fraction of the total rotation velocity, making the interpretation of $W50$ increasingly difficult and the approximation of where to measure V_{rot} in the models less well defined. Secondly, at these masses a correction for completeness is required to account for the increasingly significant number of galaxies that have no measured HI (Klypin et al. 2014). Future surveys with larger samples, more accurate velocity measurements, detailed accounting for completeness and precise understanding of the radius at which velocities are measured, are required in order to determine whether there is a statistically solid upturn in the V_{los} distribution at $V_{los} < 20$ km s^{-1}.

Bearing these caveats in mind, the comparison between the theoretical and observed velocity function highlights three points: (i) the cold dark matter model where haloes follow the widely used NFW density profile is ruled out: even by including a correction for the radius at which velocities are measured, the data could not be reconciled with a universal NFW model, (ii) the discrepancy between observations and theory can be eas-
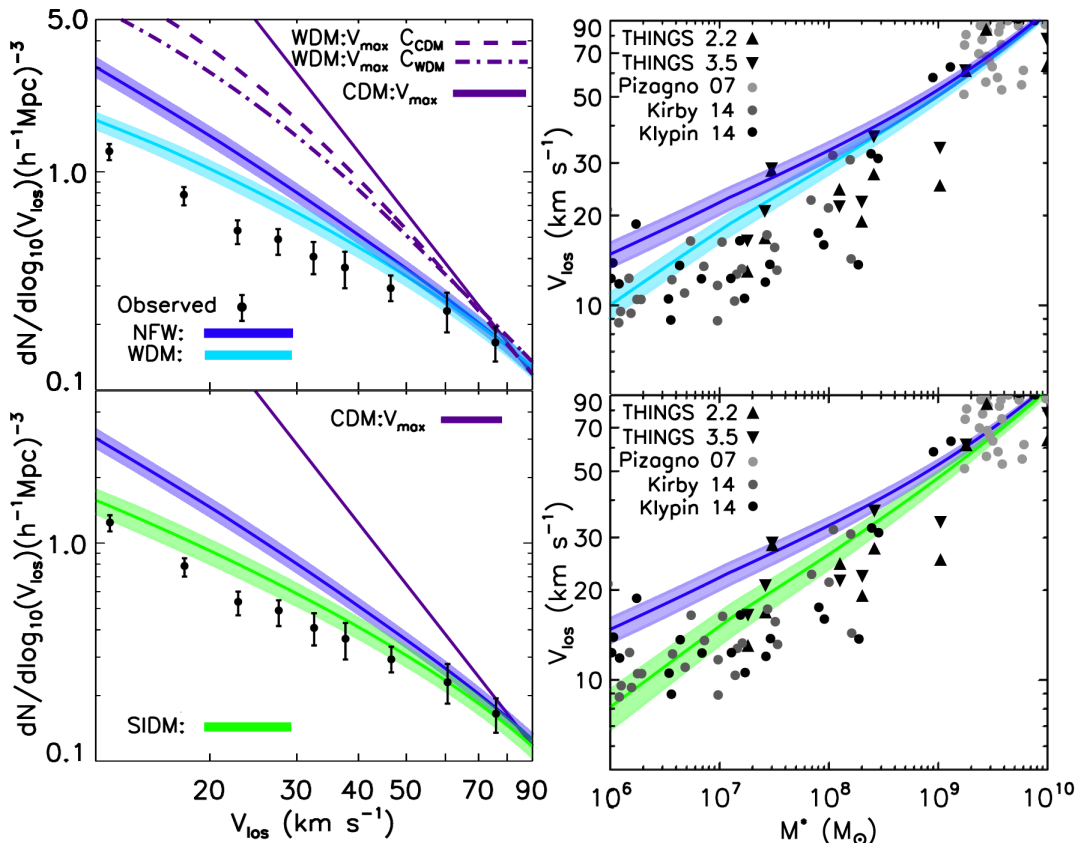
Figure 4. Top Left Panel: The velocity function, or V_{los} distribution, in a 2 KeV WDM model shown as light blue region, with velocities measured at the radius indicated in Eq. 9. In the case of velocities measured at V_{max} the resulting V_{los} distribution is shown as dashed purple line (concentraction-mass relation from CDM) or dot-dashed purple line (concentration corrected for WDM, as in Schneider et al. (2012)). The main effect of WDM particles is to change the halo mass function with respect to the CDM case. Top Right Panel: The M_{star}-V_{los} relation for WDM, with V_{los} measured between 2.2 and 3.5 disc scale-length (shaded region, with solid line representing the 2.85 scale-length measurement). Bottom Left Panel: The V_{los} distribution for cored profiles representative of the adopted SIDM models, as green area. Core sizes increase in proportion to the decrease in disc scale length from zero at $M_{star}=6\times10^{10}M_{\odot}$ to a maximum core size of 1 kpc at $M_{star}=10^{8}M_{\odot}$. Bottom Right Panel: The M_{star}-V_{los} relation for SIDM. Alternative DM models result in a flattening of the V_{los} distribution and a downward bend in the V_{los}-M_{star} relation, compared to the ΛCDM model with NFW profile, but are unable to explain observations over the full mass range.

ily explained as a manifestation of the cusp/core problem, with the mass dependent DC14 profile capturing the essence of it: a notable agreement between theory and observations is found if such a model is applied, and

(iii) the dark matter cores in galaxies formed by energetic baryonic outflows predict an upturn in the velocity function at low velocities, corresponding to the low mass galaxies regime where the energy form supernovae is less efficient at expanding haloes: such a feature may be tested with a careful comparison between theory and future updated observations.

We note that the results at the low mass end are not particularly sensitive to our disc scale-lengths, as stars become a decreasing fraction of total mass. At the high mass end, the position where the the model V_{los} intersects with the dark matter only V_{max}, is sensitive to the adopted disc scale-lengths, as well as to the assumed adiabatic contraction, but this does not affect our main results.

3.2 M_{star}-Velocity Relation

In this section, we take another perspective of the problem, exploring the relation between the velocity and stellar mass of galaxies

(Tully & Fisher 1977). Observational and systematic biases in this process will differ from biases that may exist in the velocity distribution comparison made above.

Galaxy stellar masses from large surveys (Baldry et al. 2012) can be matched to dark matter haloes (Guo et al. 2010), allowing us to derive theoretical rotation velocity for galaxies of given stellar mass at any radius. We then obtain high resolution velocity information for a sample of observed galaxies (Pizagno et al. 2007; Kirby et al. 2014; Klypin et al. 2014; Oh et al. 2008; Walter et al. 2008; de Blok et al. 2008; Oh et al. 2011) and compare observed and theoretical values of V_{los} between 2.2 and 3.5 scale lengths. To derive this region, we use the empirical relation between disc scale-lengths and M_{star} (Dutton et al. 2011a; Fathi et al. 2010).

In the right panel of Figure 2 we show results of this comparison. THINGS galaxies are plotted at both 2.2 (upward pointing triangles) and 3.5 scale-lengths (downward pointing triangles) (Walter et al. 2008; Oh et al. 2008; de Blok et al. 2008; Oh et al. 2011). At the high mass galaxies end (Pizagno et al. 2007), there is very little difference between measuring V_{los} at 2.2 and 3.5 scale-lengths. At the low mass end, the region of 2.2-3.5 disc scale-lengths is a

reasonable proxy for the radial range at which kinematics of dwarf spheroidal galaxies are measured (Kirby et al. 2014).

As shown in the right panel of Figure 2, the ΛCDM model with NFW profile (blue shaded line) predicts that dwarf galaxies with $M_{star} \sim 5 \times 10^6 - 5 \times 10^8 \, M_\odot$, should have significantly higher V_{los} than is observed, a well documented issue within the standard ΛCDM model (e.g. Read et al. 2006; Oh et al. 2011; Tollerud et al. 2014). The DC14 model (red shaded line), instead, predicts that the dark matter density profile is flattest for massive dwarf galaxies, such that the relation between V_{los}-M_{star} becomes lower than the NFW expectation at masses $10^7 < M_{star}/M_\odot < 10^9$. Moving to even lower stellar masses, the steepening of the halo profile causes the V_{los}-M_{star} relation to flatten, eventually re-joining the NFW model for galaxies with stellar masses of $M_{star} \sim 10^6 M_\odot$.

The well known independence of velocity from stellar mass observed in low mass dwarf galaxies, such as satellites of the Milky Way, Andromeda and ultrafaint dwarfs (Strigari et al. 2008; Garrison-Kimmel et al. 2014, and references therein), is therefore a feature naturally reproduced by haloes that are flattened by astrophysical processes, such as supernovae-energy-driven outflows of gas, and that retain a cuspy profile at the smallest scales, $M_{star} < 3 \times 10^6 M_\odot$ (Governato et al. 2012; Brooks & Zolotov 2014; Di Cintio et al. 2014a). The overall result is that the DC14 model can explain the observed V_{los} of dwarf galaxies over a wide range in stellar mass.

A significant caveat must be mentioned here, regarding the observed measures of galaxy velocities. For the dwarf spheroidal galaxies, the circular velocity has been approximated using $V(r_{1/2}) = \sqrt{3 \langle \sigma^2 \rangle}$, which provides a reasonable estimate at the half light radius of non-rotating, dispersion supported galaxies, minimizing the errors introduced by uncertainties of the anisotropy parameter (Walker et al. 2009; Wolf et al. 2010). This methodology has been shown to work also in non-spherically symmetric systems (Thomas et al. 2011). Systematic differences exist between these estimates of circular velocity, and those coming from rotation curve data. We therefore do not want to overstate any comparison between the predictions and observations. The purpose of the paper is to highlight ways that competing theories may be contrasted: it remains observationally challenging to test for the differences that we highlight, over the full mass range that may be required.

3.3 Alternative Dark Matter Models

Alternative dark matter particles have also been suggested as solutions to the velocity function problem (Zavala et al. 2009; Vogelsberger et al. 2012; Schneider et al. 2014; Klypin et al. 2014; Papastergis et al. 2015). Such models make different predictions for how halo density profiles vary with galaxy mass.

Here, we explore predictions for the warm dark matter (WDM) and self interacting dark matter (SIDM) models introduced in Section 2. In the top left panel of Figure 4 we plot the velocity function derived assuming a 2 KeV WDM particle, which results in a different halo mass function when compared to CDM predictions. We show this effect measuring velocities at V_{max} and using a CDM concentration-mass relation (dashed purple line). We then make adjustments for WDM concentrations (Schneider et al. 2012) including adiabatic contraction (dot-dashed purple line). Clearly, modification to the halo mass function driven by a 2 KeV particle is not enough to reconcile theory and observations, if haloes' velocities are measured at V_{max}.

Therefore we procede to analyze a WDM model which includes the universal dark matter fraction plus a stellar and a gas
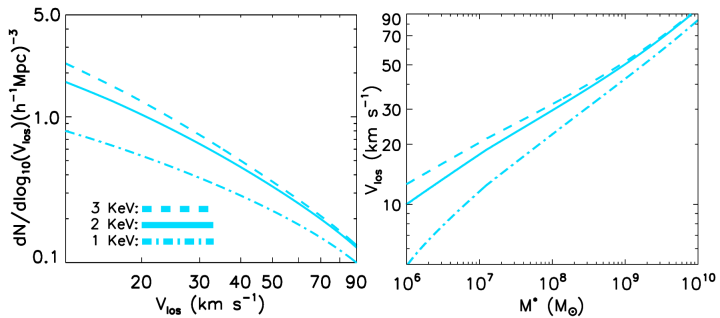
Figure 5. Left Panel: The velocity function for WDM particles of 1,2 & 3 KeV is shown as dot dashed, solid and dashed line respectively. Right Panel: The $V_{los} - M_{star}$ relation for the different WDM particle masses. The trends are the same in all cases, i.e. the V_{los} distribution bends down compared to the ΛCDM model as V_{los} become smaller, while the $V_{los} - M_{star}$ relation is steeper than the ΛCDM relation.

discs, as presented in Section 2, and in which halo velocities are measured according to Equation 9. We show the resulting velocity function in light blue in the top left panel of Figure 4. In the top right panel we show the M_{star}-V_{los} relation for WDM where the V_{los} has been measured between 2.2 and 3.5 disc scale-lengths.

The bottom left panel shows the V_{los} distribution for cored profiles (green) representative of the adopted SIDM models (Vogelsberger et al. 2012). Core sizes in the model increase in proportion to the decrease in disc scale length from zero at $M_{star} = 6 \times 10^{10} M_\odot$ to a maximum core size of 1 kpc at $M_{star} = 10^8 M_\odot$. The M_{star}-V_{los} relation for the SIDM model is shown in the bottom right panel.

Both these alternative dark matter theories result in a flattening (Zavala et al. 2009) of the V_{los} distribution in the region $30 \lesssim V_{los} \lesssim 60 \, \mathrm{km \, s^{-1}}$, as seen in Figure 4. As velocities become even smaller, however, the V_{los} distribution of these models increasingly diverge from the ΛCDM distribution, contrary to what occurs in the DC14 model. This finding is not specific to the WDM and SIDM models we show in Figure 4, but is general to any alternative DM model where core size increases relative to the virial radius, are constant at all masses, or scale with the virial radius of galaxies. No such model is able to match observations over the entire velocity range.

Alternative DM models that predict a decrease in the number of low mass haloes, and/or flattened halo density profiles even in the lowest mass galaxies, result in the velocity-M_{star} relation bending down compared to the standard ΛCDM case, better matching the velocities of observed high mass dwarf galaxies (right panels in Figure 4). However, as we move to even lower mass, such models continue to bend downward and do not match the velocity values observed for dwarf galaxies with low stellar mass. The better such models are able to account for the velocity of high mass dwarfs, the worse they fare with respect to low mass dwarfs. Our results can be generalized to rule out any model where core size increases monotonically as halo mass decreases.

3.3.1 Different WDM particle masses

We show the V_{los} distribution and $V_{los} - M_{star}$ relations for WDM particles of 1, 2 & 3 KeV as dashed, solid and dot dashed lines in Figure 5. The trends are the same in all cases, i.e. the V_{los} distribution bends down compared to the ΛCDM model as V_{los} become
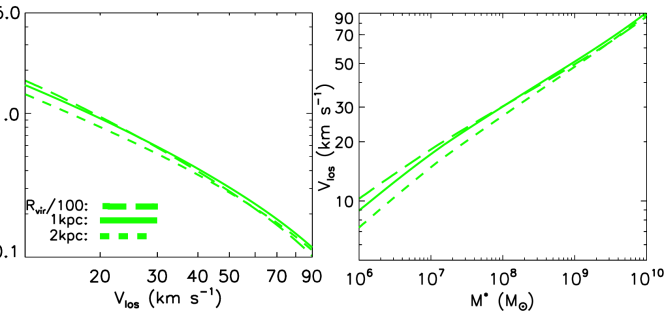
Figure 6. The V_{los} distribution (left panel) and $V_{los}-M_{star}$ relation (right panel) for various core sizes and scalings with mass. Core sizes increase linearly in proportion to the decrease in disc scale length from zero core at $M_{star}=6\times10^{10}M_\odot$ to a maximum core size of 1 (solid green line) and 2 (dashed green line) kpc at $M_{star}=10^8M_\odot$. The purple dashed line shows cores which scale in size with virial radius, core size = $R_{vir}/100$.

smaller, while the $V_{los}-M_{star}$ relation is steeper than the ΛCDM relation. None of the particle masses considered is able to reproduce observations, consistently with what has been shown previously (Klypin et al. 2014; Schneider et al. 2014). Moreover, we note that constraints from the Lyman-alpha forest indicate that WDM particles should have mass $\gtrsim 3\,\mathrm{KeV}$ (Viel et al. 2013).

3.3.2 *Different core sizes*

The parameterization of core sizes with mass, used within the adopted SIDM model in Section 3.3, mimics the main features of core dependence on halo mass for velocity dependent SIDM particles (Vogelsberger et al. 2012). In Figure 6 we show the results for different parameterizations of core sizes with mass. Core sizes increase linearly in proportion to the decrease in disc scale length from zero core at $M_{star}=6\times10^{10}M_\odot$ to a maximum core size of 1 kpc (solid green line) and 2 kpc (dashed green line) at $M_{star}=10^8M_\odot$.

Keeping a constant 1 or 2 kpc core at high masses makes very little difference (making the fit to observations at the high mass end slightly worse), so is not shown. We also show a core which scales in size with virial radius, such that core size = $R_{vir}/100$, which results in less flattening of the V_{los} distribution. None of the used parameterizations is able to reproduce the V_{los} distribution and the $V_{los}-M_{star}$ relation over the entire mass ranges.

3.4 AGN and cores in massive disc galaxies.

The large amounts of energy from AGN in the inner region of galaxies could lead to a further transformation of the inner dark matter profile (Martizzi et al. 2013). We did not include AGN in our study. Firstly, AGN activity is not likely to be significant in the mass range that is relevant to this study.

Secondly, baryons make an increasingly significant contribution to the inner density profiles at high masses: the differences in the dark matter density profile are therefore less important in high mass galaxies. We verified that a model which follows the mass dependence of the DC14 density profile at low mass, but has cored profiles for all galaxies with $M_{star}>3\times10^8M_\odot$, in order to resemble a possible AGN-driven core, does not change our results.
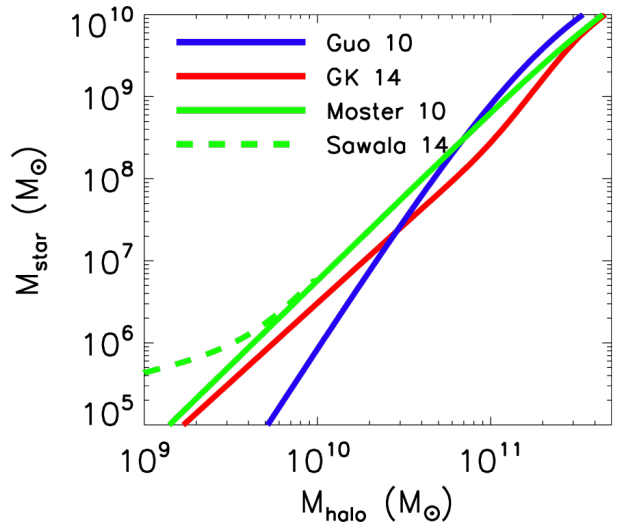
Figure 7. The M_{star} versus M_{halo} relations (Guo et al. 2010; Garrison-Kimmel et al. 2014; Moster et al. 2010; Sawala et al. 2014) that are explored. These relations cover a wide range of normalisations and slopes in the region relevant for our study.

3.5 Effects of Abundance Matching Uncertainties

In this study we relate stellar masses and halo masses using an empirical abundance matching relation (Guo et al. 2010). Several other studies provide different formulations for such relation. Here we show that the particular form of the abundance matching relation that we employ is not driving our results and conclusions.

Abundance matching relations are generally complete down to a stellar mass of few $M_{star}\sim 10^8M_\odot$, corresponding to the lower limit of large scale surveys such as SDSS (Baldry et al. 2008) and GAMA (Baldry et al. 2012). Above this mass, there is relatively little difference in the abundance matching studies (Guo et al. 2010; Moster et al. 2010; Behroozi et al. 2013), and such differences are insignificant in terms of our study. However for stellar masses below $\sim10^8M_\odot$ observational uncertainties exists and, as this is a crucial mass range in our study, we checked if using different abundance matching prescriptions affects the results at low stellar masses.

There are two recent studies that have extended the abundance matching relation to masses lower than $M_{star}\sim 10^8M_\odot$, by using the observed stellar mass function of the Local Group (Brook et al. 2014; Garrison-Kimmel et al. 2014). In the first study, Brook et al. (2014), it was shown that using the average halo mass function of simulated local groups, which is well described by a power law, implies a steep relation between M_{star}-M_{halo} in the region $10^{6.5}<M_{star}/M_\odot<10^8$. The empirically extended relation found in Brook et al. (2014) matches well the extrapolated abundance matching relation used in this paper (Guo et al. 2010).

The second study, Garrison-Kimmel et al. (2014), choses a particular collisionless simulation of the local group which has a flatter than average halo mass function, allowing the use of a flatter M_{star}-M_{halo} relation when matching haloes to the Local Group stellar mass function. It also showed that, using an even flatter M_{star}-M_{halo} relation as in Behroozi et al. (2013), the results is a severe over-estimate of the number of local group galaxies with stellar masses $10^{6.5} \lesssim M_{star}/M_\odot \lesssim 10^8$.

Considering these empirical constraints, we explore the effects of choosing flatter abundance matching relations than the one used
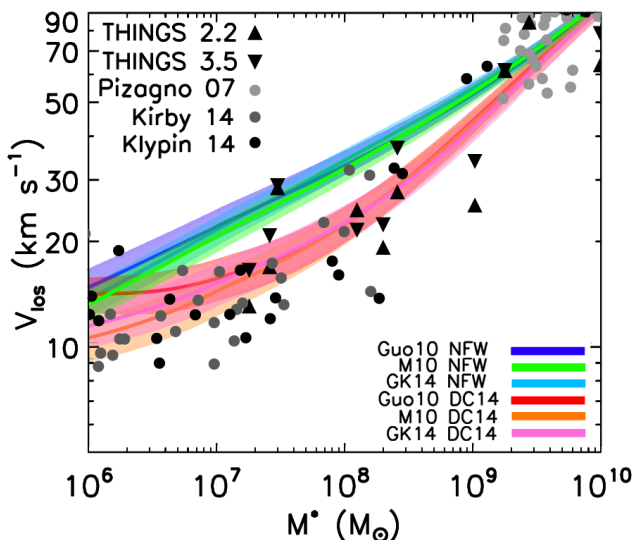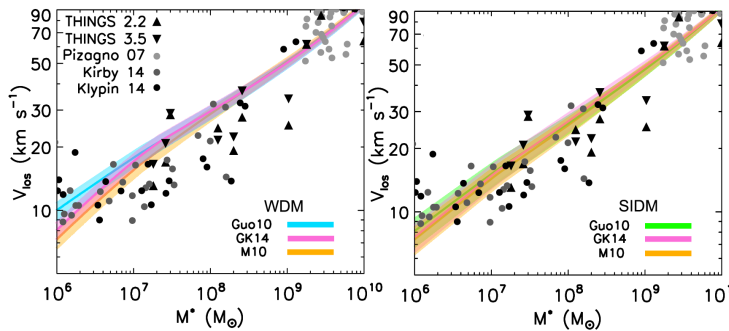
Figure 8. The M_{star}-V_{los} relations for the NFW and DC14 models, using different abundance matching relations (Guo et al. 2010; Garrison-Kimmel et al. 2014; Moster et al. 2010), which span a wide range of normalisation and slope. The conclusions of the paper are not affected: the DC14 profile still provides a very good fit to the data, for all the abundance matching relations, while the NFW profile does not match observations when the full range of dwarfs masses is considered.

Figure 9. The M_{star}-V_{los} relations for the WDM and and SIDM models, using different abundance matching relations (Guo et al. 2010; Garrison-Kimmel et al. 2014; Moster et al. 2010). A flatter relation between M_{star} and M_{halo} results in a steeper M_{star}-V_{los} relation, worsening the mismatch with observations.

in the paper. The three tested relations (Guo et al. 2010; Garrison-Kimmel et al. 2014; Moster et al. 2010), shown in Figure 7, cover a very broad range in slope and normalisation, particularly at low masses. For a halo mass of $10^{10} M_{\odot}$, there is approximately an order of magnitude difference in the matched stellar mass according to the different relations used. The velocity function relation of the DC14, NFW, SIDM and WDM models will only suffer from a negligible change when different abundance matching are applied, and therefore it is not shown here. We plot M_{star}-V_{los} using the different abundance matching relations for the NFW and DC14 models in Figure 8, and for the alternative dark matter models in Figure 9.

The most important general observation is that altering the abundance matching will alter each of the models in a consistent manner. To be specific, choosing an abundance matching relation that is flatter than the fiducial one used in the paper (Guo et al. 2010), steepens the M_{star}-V_{los} relation in all models. Thus, all models that were already too steep in the region $5 \times 10^6 < M_{star}/M_{\odot} < 3 \times 10^8$, (i.e. all but the DC14 model), worsen. The DC14 model still does very well at matching the observations in this important mass range, and the advantage over the other models is clearly maintained in full. The NFW, SIDM, and WDM models all fail at reproducing the observed M_{star}-V_{los} relation, predicting dwarf galaxies with an increasingly low V_{los} when a flatter abundance matching relation is assumed.

It may seem a little surprising that a large change in the abundance matching relation results in a relatively small change in the M_{star}-V_{los} relation. This is in part due to lower mass haloes having higher concentrations. We remind that the fact that the mass-concentration relation results in similar velocity measurements, for low mass galaxies over a range of halo masses, has been shown previously (Kravtsov 2010). This study concerns the effects of baryons in altering the haloes in which galaxies are hosted, which we implement using the DC14 model. A different proposal is that baryonic processes effectively "adjust" the halo mass function (Sawala

et al. 2014), flattening the M_{star}-M_{halo} relation. In the most important region of our study, $5 \times 10^6 < M_{star}/M_{\odot} < 3 \times 10^8$, galaxy stellar masses are matched to haloes that are well above the mass where re-ionization may render some haloes dark, $M_{halo} \sim 5 \times 10^9 M_{\odot}$ (Bullock et al. 2000), regardless of which abundance matching relation is used. The "bend" in the M_{star}-M_{halo} relation due to re-ionisation, as proposed by Sawala et al. (2014), occurs at lower masses than what is considered in this study, $M_{star} < 10^6 M_{\odot}$.

4 CONCLUSIONS

The *cusp-core* discrepancy is a challenge to the ΛCDM paradigm, which is heightened by studies showing that non-standard dark matter particles can result in cored dark matter haloes. In this paper we have highlighted how it is possible, from a theoretical point of view, to distinguish between astrophysical processes and alternative dark matter scenarios that are able to create cores in galaxies.

The key is that different models make different predictions for how core formation depends on mass. We show the signatures of these differences in galaxy populations, in particular by studying the velocity function and the Tully-Fisher relation.

Using analytic models, we have shown that the density profiles, DC14, resulting from energetic feedback processes like supernova explosions, have a particular mass dependence with a maximum core formation efficiency at $M_{star} \sim 10^{8.5} M_{\odot}$ (Di Cintio et al. 2014a,b). This value matches the peak mass of core formation occurring in hydrodynamical simulations (Stinson et al. 2013; Brook et al. 2012a). These findings allow us to create model populations of galaxies within dark matter haloes that have been affected by such energetic processes, and to compare them with models that assume a universal, steep, NFW density profile.

In agreement with previous studies, we showed that it is difficult to reconcile a model galaxy population that assumes an NFW profile for dark matter haloes with the observed velocity function of galaxies with line-of-sight velocity $V_{los} < 60$ km/s (Zavala et al. 2009; Papastergis et al. 2011; Trujillo-Gomez et al. 2011; Klypin et al. 2014; Papastergis et al. 2015), and with the observed Tully-Fisher relation of galaxies with stellar mass $\sim 10^7$-$10^9 M_{\odot}$. The mismatch holds without assuming a priori that galaxies rotation curves are tracking the maximum velocity of dark matter haloes.

By contrast, a model in which the density profile varies according to the ratio M_{star}/M_{halo}, as expected when the halo profile

is affected by baryonic outflows of gas, is able to reproduce both the velocity function and the M_{star}-velocity relation of galaxies, under plausible assumptions regarding the manner in which observations and theory are compared. Further, we show that the particular mass dependence of cores formed by baryonic outflows will leave signatures within both the velocity function and the M_{star}-velocity relation of galaxies. Specifically, the steepening of the profiles as galaxy mass decreases below $M_{star} \sim 10^{8.5} M_\odot$ results in an upturn in the velocity function for $V_{los} \lesssim 20\,\mathrm{km\,s^{-1}}$ and in a flattening of the M_{star}-velocity relation in the region $10^6 \lesssim M_{star}/M_\odot \lesssim 10^8$, both features in agreement with current data (Klypin et al. 2014).

The independence of velocity from stellar mass observed in low mass dwarf galaxies (Strigari et al. 2008; Garrison-Kimmel et al. 2014, and references therein) is thus a feature naturally reproduced by haloes that are flattened by astrophysical processes. Evidence for an observed upturn in the velocity function is more tenuous, relying on the manner in which galaxies that are devoid of gas are added to results coming from large scale surveys of HI line-widths. Further to this, an increased ratio of velocity dispersion to rotation velocity means that HI line-widths of low mass galaxies may be more difficult to interpret than in more massive galaxies.

Alternative dark matter models also make predictions for how halo density profiles vary with galaxy mass. We explored predictions from WDM and SIDM models, finding that both result in a flattening of the V_{los} distribution in the region $30 \lesssim V_{los} \lesssim 60$ $\mathrm{km\,s^{-1}}$; as velocities become even smaller, however, the V_{los} distribution of these models increasingly diverge from the ΛCDM distribution, contrary to what occurs in the DC14 model. Any model that predicts a decrease in the number of low mass haloes (such as WDM) and/or cores in the lowest mass galaxies (such as SIDM), results in the M_{star}-velocity relation better matching observations of high mass dwarf galaxies than the NFW model, but as we move to the lowest masses, such models continue to bend downward and do not match the observed velocities of the faintest dwarf galaxies. The better such models are able to account for the velocity of high mass dwarfs, the worse they fare with respect to low mass dwarfs.

These findings can be generalized to any alternative dark matter model in which core size increases monotonically as halo mass decreases, are constant at all masses, or scale with the virial radius of galaxies.

It must be noted that in this paper we did not use the distribution of gas and stars from hydrodynamical simulations, but we rather coupled the mass dependent DC14 profile with empirical galaxy scaling relations to make model galaxy populations.

In a future study we will compare HI line-widths measured directly from our simulations to the empirical $V_{max} - V_{rot}$ abundance matching relation found in Papastergis et al. (2015). We note that the hydrodynamical simulations of Governato et al. (2012) and Brooks & Zolotov (2014) included in Papastergis et al. (2015) did not match the $V_{max} - V_{rot}$ abundance matching at the low mass end, and we will explore whether this holds in our simulations and whether there are differences between simulated galaxies and empirical model for galaxy properties adopted here.

It remains a theoretical and observational challenge to compare measured velocities of observed dwarf galaxies to model predictions, particularly as the ratio of velocity dispersion to rotational velocity increases for low mass galaxies. Uncertainties associated with stellar velocity dispersions in local dSphs should be reduced thanks to GAIA satellite data (Perryman et al. 2001), and possibly also next generation 40m telescopes such as the European ELT, working with multi adaptive optic cameras (Davies & Genzel 2010). Meanwhile, the next generation of HI surveys, as we enter the era of SKA, promise high spatial resolution HI gas kinematics in a large sample of galaxies, with increased fidelity in the derivation of the velocity function (Staveley-Smith & Oosterloo 2015).

More sophisticated comparisons between observations and theory are certainly required, as are further models exploring the nature of density profiles that form under the influence of baryonic outflows; different feedback implementations, higher resolution simulations and more diverse initial conditions will likely result in an improvement of our understanding of how density profiles are modified by baryonic physics.

REFERENCES

Adams J. J., et al., 2014, ApJ, 789, 63
Agnello A., Evans N. W., 2012, ApJ, 754, L39
Amorisco N. C., Evans N. W., 2012, MNRAS, 419, 184
Baldry I. K., Glazebrook K., Driver S. P., 2008, MNRAS, 388, 945
Baldry I. K., et al., 2012, MNRAS, 421, 621
Battaglia G., Helmi A., Tolstoy E., Irwin M., Hill V., Jablonka P., 2008, ApJ, 681, L13
Behroozi P. S., Wechsler R. H., Conroy C., 2013, ApJ, 770, 57
Bode P., Ostriker J. P., Turok N., 2001, ApJ, 556, 93
Brinks E., Walter F., Ott J., 2002, in Athanassoula E., Bosma A., Mujica R., eds, Astronomical Society of the Pacific Conference Series Vol. 275, Disks of Galaxies: Kinematics, Dynamics and Peturbations. pp 57–60
Brook C. B., Di Cintio A., 2015, MNRAS, 450, 3920
Brook C. B., et al., 2011, MNRAS, pp 595–+
Brook C. B., Stinson G., Gibson B. K., Roškar R., Wadsley J., Quinn T., 2012a, MNRAS, 419, 771
Brook C. B., Stinson G., Gibson B. K., Wadsley J., Quinn T., 2012b, MNRAS, 424, 1275
Brook C. B., Di Cintio A., Knebe A., Gottlöber S., Hoffman Y., Yepes G., Garrison-Kimmel S., 2014, ApJ, 784, L14
Brooks A. M., Zolotov A., 2014, ApJ, 786, 87
Bullock J. S., Kravtsov A. V., Weinberg D. H., 2000, ApJ, 539, 517
Cannon J. M., et al., 2011, ApJ, 739, L22
Catinella B., Giovanelli R., Haynes M. P., 2006, ApJ, 640, 751
Davies R., Genzel R., 2010, The Messenger, 140, 32
Di Cintio A., Brook C. B., Macciò A. V., Stinson G. S., Knebe A., Dutton A. A., Wadsley J., 2014a, MNRAS, 437, 415
Di Cintio A., Brook C. B., Dutton A. A., Macciò A. V., Stinson G. S., Knebe A., 2014b, MNRAS, 441, 2986
Dutton A. A., Macciò A. V., 2014, MNRAS, 441, 3359
Dutton A. A., et al., 2011a, MNRAS, 410, 1660
Dutton A. A., et al., 2011b, MNRAS, 416, 322
Evans N. W., An J., Walker M. G., 2009, MNRAS, 393, L50
Fathi K., Allen M., Boch T., Hatziminaoglou E., Peletier R. F., 2010, MNRAS, 406, 1595
Ferrero I., Abadi M. G., Navarro J. F., Sales L. V., Gurovich S., 2012, MNRAS, 425, 2817
Garrison-Kimmel S., Boylan-Kolchin M., Bullock J. S., Kirby E. N., 2014, MNRAS, 444, 222
Governato F., et al., 2012, MNRAS, 422, 1231
Guo Q., White S., Li C., Boylan-Kolchin M., 2010, MNRAS, 404, 1111
Hernquist L., 1990, ApJ, 356, 359

Kannan R., Stinson G. S., Macciò A. V., Brook C., Weinmann S. M., Wadsley J., Couchman H. M. P., 2014, MNRAS, 437, 3529

Karachentsev I. D., Makarov D. I., Kaisina E. I., 2013, AJ, 145, 101

Kirby E. N., Bullock J. S., Boylan-Kolchin M., Kaplinghat M., Cohen J. G., 2014, MNRAS, 439, 1015

Klypin A., Karachentsev I., Makarov D., Nasonova O., 2014, preprint, (arXiv:1405.4523)

Kravtsov A., 2010, Advances in Astronomy, 2010

Kroupa P., 2002, Science, 295, 82

Laporte C. F. P., Walker M. G., Peñarrubia J., 2013, MNRAS, 433, L54

Macciò A. V., Paduroiu S., Anderhalden D., Schneider A., Moore B., 2012, MNRAS, 424, 1105

Martin C. L., Shapley A. E., Coil A. L., Kornei K. A., Bundy K., Weiner B. J., Noeske K. G., Schiminovich D., 2012, ApJ, 760, 127

Martizzi D., Teyssier R., Moore B., 2013, MNRAS, 432, 1947

Maxwell A. J., Wadsley J., Couchman H. M. P., 2015, preprint, (arXiv:1505.00825)

Merritt D., Graham A. W., Moore B., Diemand J., Terzić B., 2006, AJ, 132, 2685

Moore B., 1994, Nature, 370, 629

Moster B. P., Somerville R. S., Maulbetsch C., van den Bosch F. C., Macciò A. V., Naab T., Oser L., 2010, ApJ, 710, 903

Murray N., Quataert E., Thompson T. A., 2010, ApJ, 709, 191

Murray S. G., Power C., Robotham A. S. G., 2013, Astronomy and Computing, 3, 23

Navarro J. F., Eke V. R., Frenk C. S., 1996a, MNRAS, 283, L72

Navarro J. F., Frenk C. S., White S. D. M., 1996b, ApJ, 462, 563

Obreja A., Brook C. B., Stinson G., Domínguez-Tenreiro R., Gibson B. K., Silva L., Granato G. L., 2014, MNRAS, 442, 1794

Obreschkow D., Ma X., Meyer M., Power C., Zwaan M., Staveley-Smith L., Drinkwater M. J., 2013, ApJ, 766, 137

Oh S.-H., de Blok W. J. G., Walter F., Brinks E., Kennicutt Jr. R. C., 2008, AJ, 136, 2761

Oh S.-H., de Blok W. J. G., Brinks E., Walter F., Kennicutt Jr. R. C., 2011, AJ, 141, 193

Oh S.-H., et al., 2015, AJ, 149, 180

Papastergis E., Martin A. M., Giovanelli R., Haynes M. P., 2011, ApJ, 739, 38

Papastergis E., Cattaneo A., Huang S., Giovanelli R., Haynes M. P., 2012, ApJ, 759, 138

Papastergis E., Giovanelli R., Haynes M. P., Shankar F., 2015, A&A, 574, A113

Peñarrubia J., Pontzen A., Walker M. G., Koposov S. E., 2012, ApJ, 759, L42

Perryman M. A. C., et al., 2001, A&A, 369, 339

Pizagno J., et al., 2007, AJ, 134, 945

Pontzen A., Governato F., 2012, MNRAS, 421, 3464

Read J. I., Wilkinson M. I., Evans N. W., Gilmore G., Kleyna J. T., 2006, MNRAS, 367, 387

Sawala T., et al., 2014, preprint, (arXiv:1404.3724)

Schneider A., Smith R. E., Macciò A. V., Moore B., 2012, MNRAS, 424, 684

Schneider A., Anderhalden D., Macciò A. V., Diemand J., 2014, MNRAS, 441, L6

Staveley-Smith L., Oosterloo T., 2015, preprint, (arXiv:1506.04473)

Stinson G. S., Brook C., Macciò A. V., Wadsley J., Quinn T. R., Couchman H. M. P., 2013, MNRAS, 428, 129

Strigari L. E., Bullock J. S., Kaplinghat M., Simon J. D., Geha M., Willman B., Walker M. G., 2008, Nature, 454, 1096

Strigari L. E., Frenk C. S., White S. D. M., 2014, preprint, (arXiv:1406.6079)

Swaters R. A., Sancisi R., van Albada T. S., van der Hulst J. M., 2009, A&A, 493, 871

Thomas J., et al., 2011, MNRAS, 415, 545

Tollerud E. J., Boylan-Kolchin M., Bullock J. S., 2014, MNRAS, 440, 3511

Tremaine S., Gunn J. E., 1979, Physical Review Letters, 42, 407

Trujillo-Gomez S., Klypin A., Primack J., Romanowsky A. J., 2011, ApJ, 742, 16

Tully R. B., Fisher J. R., 1977, A&A, 54, 661

Viel M., Becker G. D., Bolton J. S., Haehnelt M. G., 2013, Phys. Rev. D, 88, 043502

Vogelsberger M., Zavala J., Loeb A., 2012, MNRAS, 423, 3740

Vogelsberger M., Zavala J., Simpson C., Jenkins A., 2014, MNRAS, 444, 3684

Walker M. G., Peñarrubia J., 2011, ApJ, 742, 20

Walker M. G., Mateo M., Olszewski E. W., Peñarrubia J., Wyn Evans N., Gilmore G., 2009, ApJ, 704, 1274

Walter F., Brinks E., de Blok W. J. G., Bigiel F., Kennicutt Jr. R. C., Thornley M. D., Leroy A., 2008, AJ, 136, 2563

Weiner B. J., et al., 2009, ApJ, 692, 187

Wolf J., Martinez G. D., Bullock J. S., Kaplinghat M., Geha M., Muñoz R. R., Simon J. D., Avedo F. F., 2010, MNRAS, 406, 1220

Zavala J., Jing Y. P., Faltenbacher A., Yepes G., Hoffman Y., Gottlöber S., Catinella B., 2009, ApJ, 700, 1779

Zwaan M. A., Meyer M. J., Staveley-Smith L., 2010, MNRAS, 403, 1969

de Blok W. J. G., Walter F., Brinks E., Trachternach C., Oh S.-H., Kennicutt Jr. R. C., 2008, AJ, 136, 2648